ANALYZING SCENE GEOMETRIES FOR STEREO PUSHBROOM IMAGERY

Michal Jama, Graduate Research Assistant
Dr. Chris Lewis, Associate Professor
Dr. Dale Schinstock, Associate Professor
Autonomous Vehicle Systems Lab
Kansas State University
Manhattan, KS 66506
mjama@ksu.edu
clewis@ksu.edu
dales@ksu.edu

ABSTRACT

Bundle Adjustment (BA) is an important step in deriving high quality terrain products from stereo pairs of satellite imagery. Most satellites use pushbroom cameras for image acquisition due to improved signal to noise ratio. The BA process is not as well constrained for pushbroom imagery as it is for frame cameras. Due to the loss of perspective along track additional degrees of freedom are present in BA. Usually Ground Control Points (GCPs) are used to provide necessary constraints. However in order to reduce cost and allow automated processing GCPs are being excluded from BA and Path Control Points (PCPs) are used instead. Without ground control, scene geometry and the technique for describing the camera's path become more critical. In this paper we study the effects that different scene geometries have on the accuracy of the reconstructed terrain. A method to identify degrees of freedom is developed and utilized to constraints of five commonly used geometries. Theoretical results are supplemented with the numerical analysis of the geometries used in satellite and aerial imagery.

INTRODUCTION

Bundle Adjustment (BA) is an algorithm commonly utilized in attempts to improve camera position and orientation estimates for stereo imagery. This is useful as a precursor to other processes such as orthorectification, terrain extraction, and other photgrammetric processes. BA was first formulated in 1958 for use in photogrammetry (Brown, 1958). Since then it has been successfully utilized by many (for example (Orun and Natarajan, 1994, Ebner et al., 1999, Bouillon et al., 2006, Li et al., 2008) and is commonly used in photogrammetry software. A significant amount of research has been directed at reducing the computational complexity of BA, for example by utilizing sparseness of the Jacobian matrix (George and Liu, 1981, Duff et al., 1989). More recently BA has gained interest in the computer vision community and has been described in books and papers (Hartley and Zisserman, 2004, Triggs et al., 2000). While some simple cases for a lack of constraints are known in BA with frame cameras (and correspondingly for pushbroom cameras) the literature is deficient in analytical descriptions of needed constraints for BA with pushbroom cameras.

BA with pushbroom imagery is more complicated than that with frame cameras, but is increasingly being used to generate terrain models in semi-automated processing of the imagery. However, the adjustments made by BA for pushbroom imagery may have degrees of freedom (DOF) beyond those commonly known for frame cameras (absolute position and scale). These additional DOF depend on the geometric relationship between the camera paths/poses used to obtain the imagery. Furthermore, the residuals after adjustment of the camera poses do not provide any indication that the true camera poses have not been recovered.

A common approach to eliminate DOF is to include additional constraints like Ground Control Points (GCPs). However, sometimes it is impossible or impractical to add GCPs (e.g. for extraterrestrial imagery (Kirk et al., 2007) or imagery of ice sheets (Korona et al., 2009)). In those cases Path Control Points (PCPs) from navigation are often used as the sole means of control. It is important to realize that BA may not be capable of improving errors in the path measurement due to the presence of DOF.

An example of a terrain reconstruction where DOF allow significant errors to be undetected by BA is presented in Fig. 1. In this simple scenario the orientation of one camera is disturbed while the orientation of the other camera and the position (paths) of both cameras remain fixed. Then BA is applied to refine the estimate of orientation for

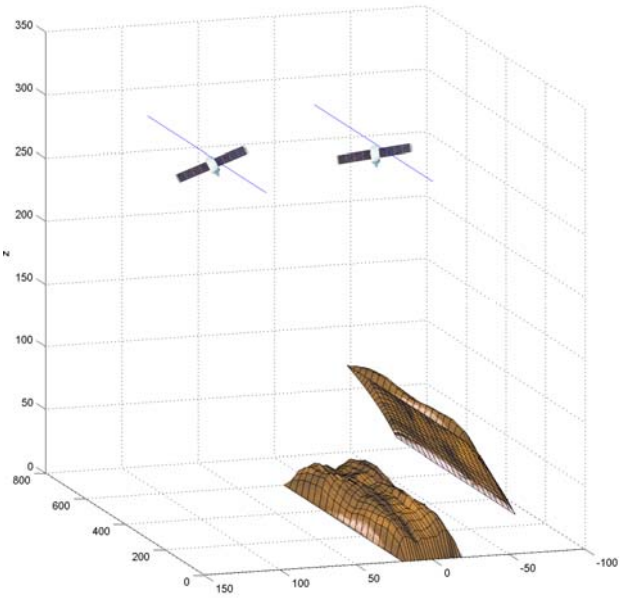

Figure 1a. Scene with the original terrain and terrain obtained by triangulation using the initial (disturbed) path parameters. The latter one is shifted and rotated. Without refinement, the triangulation error is $3.1 \cdot 10^{+0}$.

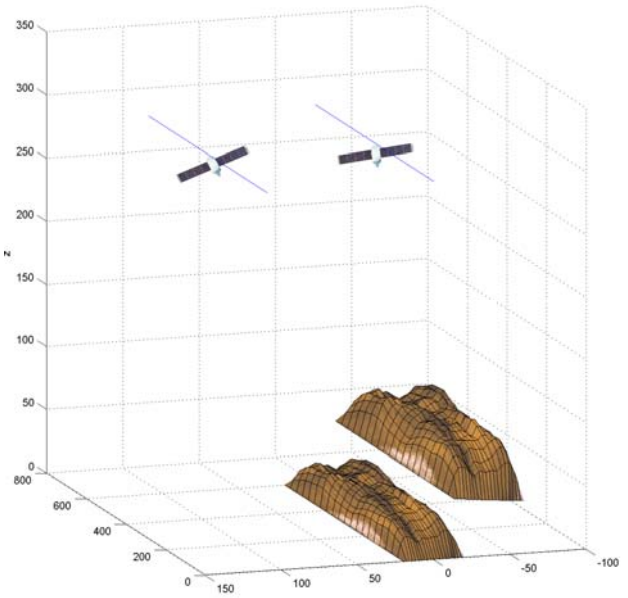

Figure 1b. Scene with the original terrain and that from triangulation after refinement using BA. The latter one remains both offset and misshapen even though the residual triangulation error is only $3.1 \cdot 10^{-17}$.

the disturbed camera while holding all other parameters fixed. For frame cameras this would constrain the well known DOF in scale and absolute position and orientation. BA converges to a cost within the counting precision of zero. However, the terrain model constructed through triangulation is a rotated, translated and warped version of the original terrain.

In this paper a method of identifying linear DOF for a given viewing geometry is described and then analyzed with numerical simulations. In the first section BA for frame and pushbroom cameras is formulated, along with an extension that allows the reduction of the parameter vector for BA through the elimination of feature locations. The second section details the mathematical formulation of the method used to identify DOF. The last section presents results of applying this method to viewing geometries common for obtaining stereo imagery with pushbroom cameras and is followed by numerical studies. The numerical studies indicate that because of the small field of view (FOV) common in high resolution satellite cameras that the mathematical DOF are no more significant that the lack of constraint posed by the small FOV. However, the numerical studies do indicate that for lower altitude, larger FOV cameras common in aerial surveys, the viewing geometries can be important in constraining BA.

BUNDLE ADJUSTMENT

This work is concerned with stereo photogrammetry from pushbroom cameras whereby a digital elevation model (DEM) is derived from two images of the same terrain captured from different vantage points. Pioneering work was performed in this area by Hoffman et al. (Hofmann et al., 1984) and Ebner and Strunz (Ebner and Strunz, 1988). Recently this topic was covered by Tiggs et al. (Triggs et al., 2000) and Hartley and Zisserman (Hartley and Zisserman, 2004).

Using camera pose (position and orientation) DEMs are produced through triangulation of corresponding features identified in both images. Like all measurements, camera pose measurements are corrupted by noise. Therefore, to improve the quality of the DEM, the camera pose estimates are adjusted to enhance scene consistency using a process called Bundle Adjustment (BA). This section details the structure of the BA algorithm to set the framework for discussion of the pitfalls of scene geometry in applying BA to stereo pushbroom imagery. General BA formulation is decribed first. Next, a method to reduce parameter vecotr size by eliminating feature coordinates is presented.

Formulation

BA adjusts all scene parameters including the camera positions, p_c, camera orientations, $\Phi_c = [\omega\ \phi\ \kappa]^T$, and feature locations in 3D, p_f, to minimize a scalar cost function. The feature locations are those associated with features identified and corresponded in two or more images, and are also known as "tie points". The cost function is typically a sum of squared errors. Individual error terms for tie points are measured in the camera's focal plane as the difference between measured location of the feature in the image and that predicted by the current state of the estimated parameters. Prediction of a feature's image location is accomplished through back-projection of p_f, into the camera's focal plane. Without lens distortion, the pinhole camera model describes how 3D points are imaged. With this model, the projection of p_f into the camera focal plane is give by

$$p_b = \begin{bmatrix} u_b \\ v_b \end{bmatrix} = \frac{f}{d_z}\begin{bmatrix} d_x \\ d_y \end{bmatrix} \tag{1}$$

where

$$d = [d_x\ d_y\ d_z]^T = R_{cr}(p_f - p_c) \tag{2}$$

and R_{cr} is a rotation matrix transforming vectors from feature p_f coordinate frame to the camera coordinate frame and defined by the camera orientation Φ_c as

$$R_{cr} = \begin{bmatrix} c_\phi c_\kappa & c_\omega s_\kappa + s_\omega s_\phi c_\kappa & s_\omega s_\kappa - c_\omega s_\phi c_\kappa \\ -c_\phi s_\kappa & c_\omega c_\kappa - s_\omega s_\phi s_\kappa & s_\omega c_\kappa + c_\omega s_\phi s_\kappa \\ s_\phi & -s_\omega c_\phi & c_\omega c_\phi \end{bmatrix}. \tag{3}$$

Here $c_* = \cos(*)$ and $s_* = \sin(*)$. The back-projection error between an observed feature, p_m, and its prediction, p_b, is given by

$$e = p_m - p_b = \begin{bmatrix} u_m \\ v_m \end{bmatrix} - \begin{bmatrix} u_b \\ v_b \end{bmatrix} = \begin{bmatrix} \partial u \\ \partial v \end{bmatrix}. \tag{4}$$

The scalar cost function measuring the scene consistency is the sum of squared back projection errors,

$$C = c^T c, \tag{5}$$

where, for m images with n tie points, the cost vector is

$$c = [e_1^T \ \dots \ e_m^T] \tag{6}$$

where $e_i = [e_{1,i}^T \ \dots \ e_{n,i}^T]^T$ for $i = 1 \dots m$. Here, for simplicity, it is assumed that all n tie points are observed in all m cameras. For n tie points and m cameras, if we define the vector of parameters to be estimated as

$$k = [p_{f_1}^T \ \dots \ p_{f_n}^T\ p_{c_1}^T\ \Phi_{c_1}^T \ \dots \ p_{c_m}^T\ \Phi_{c_m}^T]^T, \tag{7}$$

then combining equations (1), (2), (3), (4) and (6) and plugging the result into (5) provides a scalar cost as a function of the scene parameters, $C = C(k)$.

Unlike frame cameras which capture an entire image in a single pose, pushbroom cameras sweep out images by traveling through space. Each image line is acquired from a slightly different pose. Therefore, pose parameters associated with each image are a function of image line number or time, t. In this paper we express each camera pose parameter as a nominal path plus a time dependent offset. The offset is modeled as a second order polynomial

in t whose coefficients are adjusted by BA. The camera pose is given by,

$$\begin{bmatrix} p_c(t) \\ \phi_c(t) \end{bmatrix} = \begin{bmatrix} x_0(t) + \alpha_x t^2 + \beta_x t + \gamma_x \\ y_0(t) + \alpha_y t^2 + \beta_y t + \gamma_y \\ z_0(t) + \alpha_z t^2 + \beta_z t + \gamma_z \\ \omega_0(t) + \alpha_\omega t^2 + \beta_\omega t + \gamma_\omega \\ \phi_0(t) + \alpha_\phi t^2 + \beta_\phi t + \gamma_\phi \\ \kappa_0(t) + \alpha_\kappa t^2 + \beta_\kappa t + \gamma_\kappa \end{bmatrix} \tag{8}$$

where the nominal trajectories $x_0(t)$, $y_0(t)$, $z_0(t)$, $\omega_0(t)$, $\phi_0(t)$ and $\kappa_0(t)$ are assumed to be known measurements provided by a navigation system. The parameter vector k is then expanded to include the polynomial coefficients,

$$k = \left[p_{f_1}^T \cdots p_{f_n}^T \left[\alpha_{x_1} \cdots \gamma_{\kappa_1}\right] \cdots \left[\alpha_{x_m} \cdots \gamma_{\kappa_m}\right]\right]^T. \tag{9}$$

The necessary addition of these path parameters significantly decreases the constraints on the scene geometry as compared to BA for frame cameras.

Adding additional constraints such as Ground Control or Path Control Points, (GCPs or PCPs), to BA is achieved by adding elements, similar to (4), to the cost vector c. Ground control and path control measurements have different variance than back-projection errors, therefore a weighting matrix is defined using the inverse covariance to adjust for their relative significance. The scalar cost then becomes,

$$C = c^T W c, \tag{10}$$

The cost function (10) is non-linear w.r.t. the vector of parameters k. Therefore an iterative algorithm is used to find a k that minimizes the cost function. The standard approach for BA utilizes the Levenberg-Marquardt (LM) algorithm which is a hybrid between gradient descent and Newton methods. At each update step the incremental adjustment to k in the LM algorithm is computed using

$$\delta_k = -\left(J^T W J + \lambda I\right)^{-1} J^T W c \tag{11}$$

where $J = \dfrac{\partial c}{\partial K}$ is the Jacobian matrix and λ is the LM damping factor, which varies during minimization and tends to zero as a minimum is approached.

In summary, BA is an iterative algorithm that seeks to minimize the cost function $C(k)$ by varying elements of the parameter vector k. Because the camera poses and 3D feature coordinates are elements of k, BA can be conceptualized as simultaneous adjustment of camera positions and feature coordinates to minimize the difference between the measured feature coordinates in the images and those predicted by projecting the 3D coordinates into the focal planes of the cameras. While additional control measurements can be utilized in BA to help constrain the minimization, the inherent lack of constraints in pushbroom imagery necessitates careful consideration of the geometry used in image acquisition.

Elimination of Features from the Parameter Vector

The 3D positions of terrain features can be eliminated from the parameter vector for BA using triangulation. In triangulation the feature positions are found using the camera positions and orientations and the measured image coordinates of the features. If triangulation is formulated as a differentiable function of the other parameters then the feature positions become dependent variables, and can be removed from the parameter vector. Identification of the degrees of freedom by a method described in the next sections of this paper is greatly simplified by the elimination of features from the parameter vector.

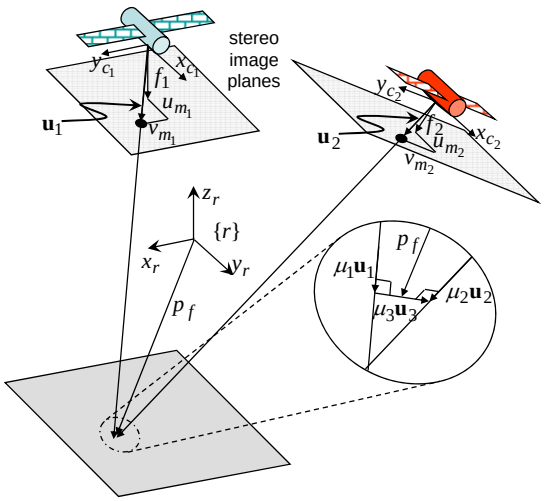

Figure 1. Triangulation using the closest point of approach of two lines.

Several methods exist for triangulation, including BA with the camera positions and orientations held constant, which is an iterative process. However we seek a closed form solution to triangulation. Specifically, the method used here is to take the feature location as the midpoint of the line between the closest points of approach for two lines. The two lines are defined using the camera positions and orientations and the feature image coordinates as shown in Fig. 1. The closest points of approach are determined by finding the mutual perpendicular for the two lines.

The development of the triangulation equations given here is based on an intuitive geometric description. First two vectors from the focal points of the images to the measured feature locations in the image plane are found using the following equation,

$$\mathbf{u}_i = \mathbf{R}_{rc_i}\begin{bmatrix} u_{m_i} \\ v_{m_i} \\ f_i \end{bmatrix} - \mathbf{R}_{rc_i}\begin{bmatrix} u_{m_i} \\ v_{m_i} \\ f \end{bmatrix}, \qquad i = 1,2 \tag{12}$$

where $\mathbf{R}_{rc_i}$ is the transpose of $\mathbf{R}_{c_i r}$ in (3). A mutual perpendicular to $\mathbf{u}_1$ and $\mathbf{u}_2$ is given by the cross product, $\mathbf{u}_3 = \mathbf{u}_1 \times \mathbf{u}_2$. A vector loop can be written that uses the two camera positions, the three pointing vectors, and three to-be-determined scalars (μ_1, μ_2, μ_3) as follows:

$$\mathbf{p}_{c_1} - \mathbf{p}_{c_2} = \mu_1\mathbf{u}_1 + \mu_3\mathbf{u}_3 - \mu_2\mathbf{u}_2 \tag{13}$$

Solving for μ_1, μ_2, μ_3 and setting $\mathbf{p}_f$ to be a midpoint of a line perpendicular to both $\mathbf{u}_1$ and $\mathbf{u}_2$ we get

$$\mathbf{p}_f = \mathbf{p}_{c_1} + \mu_1\mathbf{u}_1 + \frac{\mu_3\mathbf{u}_3}{2} \tag{14}$$

Plugging (14) into (2) removes the dependency of the cost function on the feature locations, making it only a function of the camera poses and constants. Thus the elements of the parameter vector are reduced to the parameters associated with the camera poses.

IDENTIFYING DEGREES OF FREEDOM

In this section, an approach is developed for identifying linear degrees of freedom in the BA process that do not change the minimal cost of a solution. First the problem is stated and analyzed mathematically. Then a process is described to perform the analysis needed to identify degrees of freedom for particular scene geometries.

Mathematical Problem Statement and Method Development

We are interested in finding the set of directions, s_i, in the parameter space along which we can move from the minimum without changing the cost. In other words we wish to find the directions that satisfy

$$C(k_{min}) = C(k_{min} + \varepsilon s_i), \tag{15}$$

for reasonably large ε. An ad hoc search for such a space is not feasible. We therefore need to narrow the possibilities for degrees of freedom using some analysis of the problem.

We will denote the gradient and Hessian of $C(k)$ at k_{min} respectively as g and G. The curvature of $C(k_{min})$ along the line $k_{min} + \varepsilon s$ is then $s^T G s$. It is well known (Fletcher, 2000) that a zero gradient and a non-negative curvature are necessary conditions for the existence of a minimum. Mathematically, these necessary conditions are

$$g = 0, \tag{16}$$

and

$$s^T G s \geq 0, \forall s. \tag{17}$$

Also, it is well known (Fletcher, 2000) that a sufficient condition for the existence of a strict and isolated local minimum is

$$s^T G s > 0, \forall s. \tag{18}$$

If we are at a minimum (i.e. (16) and (17) are satisfied) then the vectors satisfying (15) necessarily lie in the space not satisfying (18). The only difference between the set of vectors satisfying (17) and those satisfying (18) are those for which $s^T G s = 0$, which is a null space of G. It can be shown that any vector not satisfying (18) must lie in the null space defined by zero eigenvalues of G. Therefore the search for directions defined in (15) can be limited to vectors in the space spanned by the zero eigenvalues of G.

It should be noted that being in the null space of G is only a necessary condition for a vector to satisfy (15) when at a minimum. This is true because (18) is only a sufficient condition not a necessary and sufficient condition for an isolated minimum. Therefore the null space must be explored further to identify degrees of freedom.

For the sum of squares cost function, the problem of finding the Hessian G is significantly easier if the cost is zero. In general computing the Hessian involves finding the second partial derivatives of the cost function w.r.t. the parameters. However, if the cost is zero we only need to compute the first order derivatives associated with the Jacobian. It can be shown that for the sum of squares cost function the Hessian can be expressed as

$$G = 2J^T J + 2\sum_{i=1}^{m} c(k)\nabla^2 c(k), \tag{19}$$

The second term of this equation is zero if the cost is zero. The procedure we follow to search for degrees of freedom in a particular geometry is described by the following steps:

1. Form a simulated scene with true zero cost.
2. Compute the Jacobian, and Hessian (using $G = 2J^T J$).
3. Compute the zero eigenvalues of G and their corresponding normalized eigenvectors (e.g. using singular value decomposition (SVD)).
4. Test each of the directions given by these eigenvectors by moving along them from the zero cost solution while computing the cost. If the cost remains zero over a large range then consider it a degree of freedom and eliminate it from the space left to consider.
5. If the number of degrees of freedom identified is less than size of the null space minus one then it is still possible that a degree of freedom(s) lies in the set of vectors not eliminated from the search. Therefore, if possible, formulate a method to search this space in more detail.

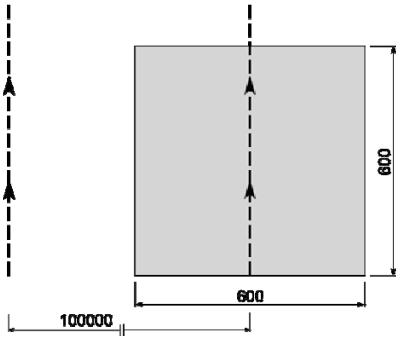

Figure 2a. Geometry 1, camera on the right is nadir looking, camera on the left looks to the side

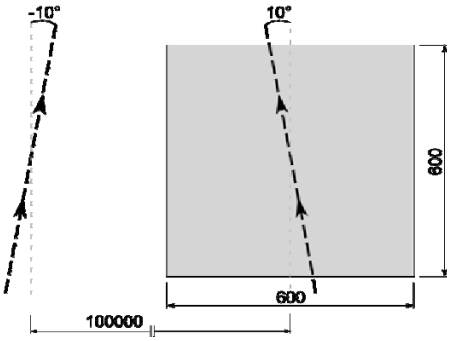

Figure 2b. Geometry 2, camera on the right is nadir looking, camera one the left looks to the side. Both cameras look at the terrain center in the center point of their paths.

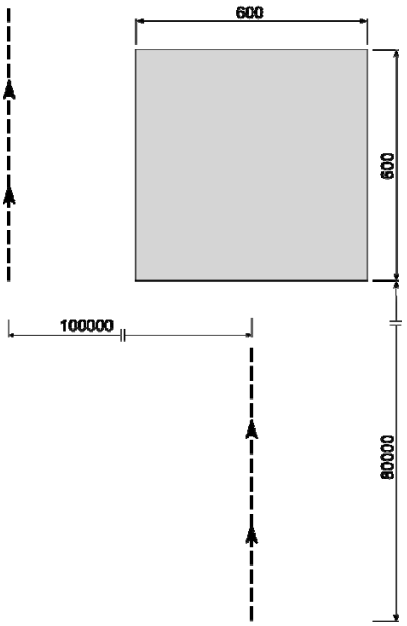

Figure 2c. Geometry 3, camera on the bottom is fore-looking, camera on the left looks to the side.

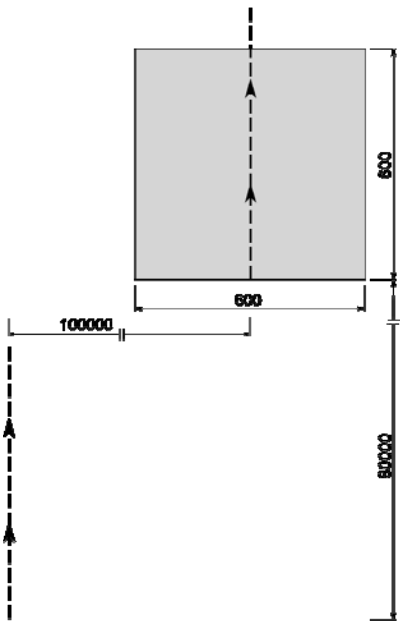

Figure 2d. Geometry 4, camera on the right is nadir-looking; camera on the bottom is fore and to the side looking.

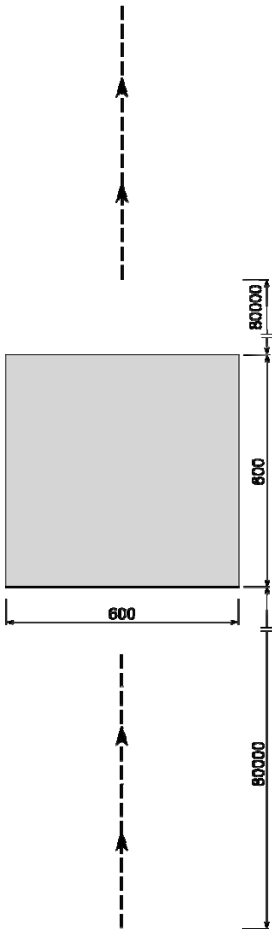

Figure 2e. Geometry 5, camera on the bottom fore-looking; camera on the top aft-looking

NUMERICAL ANALYSIS

In this section the relationship between scene geometry and BA accuracy is investigated. First five viewing candidate geometries are presented. Then, the degrees of freedom in each of these geometries are identified employing the methods developed in the previous section. A formulation of BA with a reduced parameter space is described which is applied on simulated imagery to investigate the impact scene geometry can have on BA accuracy. The results of these simulations are presented and conclusions draw from their results.

Simulation Setup

In order to perform BA we need two or more views. For the purpose of simulations we investigated five scene geometries (presented in Fig. 2), each containing two camera paths. They describe different possibilities of obtaining

Table 1. Degrees of freedom for different geometries. Top rows correspond to holding one camera fixed, allowing another one to change pose (position and orientation). Bottom rows correspond to holding both positions fixed, while allowing both orientations to be changed.

		1	*2*	*3*	*4*	*5*
Single camera *pose* fixed	*Nr of zero eigenvalues*	*3*	*0*	*0*	*0*	*1*
	Nr of degrees of freedom	*3*	*0*	*0*	*0*	*1*
Both camera *positions* fixed	*Nr of zero eigenvalues*	*1*	*0*	*0*	*0*	*1*
	Nr of degrees of freedom	*1*	*0*	*0*	*0*	*1*

stereo imagery and simulate real world conditions. In geometry 1 the first camera is nadir looking and the other gazes to the side. This arrangement is a very common way of obtaining stereo imagery when only a single instrument is present on-board the orbiter (e.g. HiRISE, LROC) and therefore two passes over the object are needed. Geometry 2 is similar to geometry 1 except that camera paths are not parallel. This is a path expected for imagery at high latitudes (i.e. close to the poles). Geometries 3 and 4 present cases where the camera paths are shifted along and/or across track. In Geometry 5 one camera is fore-looking and another is aft-looking. This geometry depicts another common way of obtaining stereo images from what have come to be known as "terrain cameras" (e.g. MOMS-02 (Ackermann et al., 1991) or SPOT5 (Gleyzes et al., 2003)). This geometry has the advantage of obtaining the image pair with very small temporal displacements since both images are captured on the same orbit.

In the method developed earlier, degrees of freedom are found based on the eigenvalue decomposition of the Hessian matrix computed at the solution. The Hessian matrix is $l \times l$, where l is the number of parameters included in the vector k . In the standard BA formulation the vector k contains feature parameters along with pose parameters. Since only the pose parameters are of interest when identifying degrees of freedom we eliminate features from the vector k . Triangulation, as described at the beginning of this paper, facilitates elimination of features from k leaving only camera pose parameters.

It is well known that without any external control, like GCPs or PCPs, BA cannot recover absolute position and orientation of the camera, but can only solve for relative position with an unknown scale factor. Therefore allowing both cameras' parameters to vary without external control results in at least seven degrees of freedom associated with identical motions of the two cameras and a scaling of all of the camera positions. To eliminate these obvious degrees of freedom scenarios were investigated with some of camera's pose parameters fixed. In the first scenario the position and orientation of one camera is fixed, while the second camera pose is adjusted. This first scenario eliminates the six degrees of freedom where both cameras experience simultaneous and identical translation and rotation along with the scene. It also fixes scale since the length of the path now defines the scale of the scene. In the second scenario the positions of both cameras are fixed while their orientations are adjusted by BA. This scenario also eliminates six degrees of freedom, three for each of the camera's positions, but will isolate any degree of freedom associated with only rotation. Again, scale is set by the length of the paths and the distance between the paths. To further simplify the analysis only constant camera pose perturbations are allowed, instead of quadratic perturbations given in (8). Higher order perturbation increase the degree of freedom independent of the viewing geometry. Our formulation is consistent with the underlying statement of the problem (15). With these assumptions, the vectors k used to analyze scenario 1 and scenario 2 are $k = [\gamma_{\omega}, \gamma_{\phi}, \gamma_{\kappa}, \gamma_{\omega}, \gamma_{\phi}, \gamma_{\kappa}]^T$ and $k = [\gamma_{\omega_1}, \gamma_{\phi_1}, \gamma_{\kappa_1}, \gamma_{\omega_2}, \gamma_{\phi_2}, \gamma_{\kappa_2}]^T$ respectively.

Identified Degrees of Freedom

For each geometry an artificial scene is generated. The true locations of a set of well dispersed features is projected into the pushbroom images from the true camera paths, giving a scene with zero cost. The Jacobian for the reduced parameter vector, the Hessian ($G = J^T J$), and the SVD of the Hessian are calculated. The computation is performed for both scenarios. Any eigenvector associated with an eigenvalue of zero is taken as a candidate for a degree of freedom of the geometry. To evaluate the candidate degrees of freedom, ξ_i, the camera path is perturbed from the true camera path, $[p_Q(t)^T \quad \phi_Q(t)^T]^T$, in the direction of the candidate. In this case the camera path is given by

Table 2. RMS of terrain error for 100 simulation runs for satellite imagery with assumed image noise of 0.5 pixel and path noise of [5m, 5m, 5m, $15e^{-6}$rad, $15e^{-6}$rad, $15e^{-6}$rad]

	Geometry									
	1		***2***		***3***		***4***		***5***	
	Init	*BA*	*Init*	*BA*	*Init*	*BA*	*Init*	*BA*	*Init*	*BA*
x	*3.76*	*3.09*	*3.02*	*2.04*	*4.44*	*4.19*	*3.89*	*3.14*	*3.79*	*3.11*
y	*4.24*	*2.92*	*4.19*	*4.20*	*3.93*	*2.88*	*3.78*	*3.01*	*2.81*	*2.59*
z	*18.47*	*15.82*	*15.74*	*16.43*	*14.53*	*12.95*	*15.65*	*13.75*	*13.50*	*11.95*
avg	***8.82***	***7.28***	***7.65***	***7.56***	***7.63***	***6.67***	***7.77***	***6.64***	***6.70***	***5.89***

$$\begin{bmatrix} p_c(t) \\ \phi_c(t) \end{bmatrix} = \begin{bmatrix} p_0(t) \\ \phi_0(t) \end{bmatrix} + \varepsilon \xi_i \tag{20}$$

where ε is a scale factor. This makes the cost a function of the scale factor, $C(k) = C(\varepsilon \xi_i) = C(\varepsilon)$. If the cost remains zero over a wide range of ε, then the candidate is taken as a degree of freedom for the geometry. If all of these candidates are degrees of freedom then the number of degrees of freedom is clear, and so is their orthogonal set of directions. However, if there is more than one candidate that did not pass the degree of freedom test then it is still possible for degrees of freedom to lie in the space defined by the null vectors.

MATLAB software was used in all computations. In order to increase precision Variable Precision Arithmetic (VPA) was used with 1000 decimal digits during Jacobian computation and the singular value decomposition of the Hessian matrix. This aided in distinguishing between eigenvalues that are truly zero and those that are merely small. To ensure accuracy the Jacobian was calculated using symbolically developed equations rather than a numerical method. These equations are very lengthy and cannot be presented here.

Results of analysis are presented in **Table 1**. Consider the first scenario. For geometry 1 three degrees of freedom were identified, namely along Y, Z, and ω. This convenient and commonly used geometry is poorly constrained. For geometry 5 a single degree of freedom, along X, was identified. This along path direction is coincidently the most poorly known for PCP measurements from the navigation systems of many satellites. Now consider the second scenario. Additional degrees of freedom were found again in both geometry 1 and geometry 5. For geometry 1 the degree of freedom was again found to be along ω. For geometry 5 the degree of freedom exist for simultanous rotation along ω in the same direction of both cameras. In summary, three degrees of freedom were found for geometry 1 and two degrees of freedom were found for geometry 5. The other geometries are mathematically constrained (i.e. a single isolated minimum exists).

Simulations of Satellite Imagery

Computer simulations were performed to assess the influence of degrees of freedom on the accuracy of BA. A simulation was again developed for this analysis. First a terrain model consisting of 512 points was created. Then, using one of the imaging geometries and a simple camera model resembling the QuickBird camera, (Salvini et al., 2004, DigitalGlobe, 2009), artificial images were generated. At this point, error-free terrain reconstruction was possible through triangulation. Next white Gaussian noise with a standard deviation of 0.5 pixels was added to the images to simulate feature detection errors in real images. Finally colored noise was used to disturb path measurements. The standard deviation of the noise added to path measurements was 5m for position and $15e^{-6}$ rad for orientation. At this point, due to added noise, terrain reconstructed by the triangulations is significantly different from the original terrain. Ten evenly distributed path measurements were selected and used as PCPs. These artificial noisy images and PCPs provide input to the BA algorithm. This BA algorithm adjusts both camera poses and was allowed to run until convergence. RMS of the difference between BA reconstructed terrain and the original terrain defines the performance measure of the accuracy of BA. The above procedure was repeated 100 times and the average results are presented **Table 2**.

In all cases the terrain reconstructed by BA is closer to the original terrain than the terrain obtained by initial triangulation and the accuracy gained through applying BA is similar for all geometries. There is no clearly visible advantage in using a mathematically constrained geometry over one that is constrained. This result appears to refute the previous analysis. To understand the discrepancy between the existence of degrees of freedom and BA's performance additional tests were performed.

Table 3. RMS of terrain error for 100 simulation runs for aerial imagery with assumed image noise of 0.1 pixel and path noise of [10m, 10m, 10m, $5e^{-3}$rad, $5e^{-3}$rad, $5e^{-3}$rad]

	RMS Error				**Shape Error**			
	Geo 1		***Geo 2***		***Geo 1***		***Geo 2***	
	Init	*BA*	*Init*	*BA*	*Init*	*BA*	*Init*	*BA*
x	*6.08*	*5.85*	*6.08*	*5.64*	*0.24*	*0.21*	*0.28*	*0.01*
y	*6.95*	*5.53*	*6.99*	*3.99*	*2.01*	*1.56*	*2.04*	*0.05*
z	*19.35*	*15.19*	*19.54*	*4.51*	*0.11*	*0.09*	*0.27*	*0.03*
avg	***10.79***	***8.86***	***10.87***	***4.71***	***0.79***	***0.62***	***0.86***	***0.03***

Typical satellite imagery is from high altitude with a very narrow field of view (FOV). These high aspect ratios are an additional source of ill conditioning for BA which swamp out the geometric effects we address. On the other hand pushbroom imagery from air vehicles has significantly lower aspect rations due to both lower altitudes and wider FOV cameras. Examples of pushbroom cameras used in aerial missions include ADS40, ADS80 from Leica Geosystems (Fricker, 2001, Sandau, 2010) or High Resolution Stereo Camera (HRSC) (Neukum, 1999).

A second simulation was performed using a model of an aerial camera similar to HRSC with a FOV increased from 12 to 20 degrees. The focal length was 165mm and the pixels size was 6,5um and the flight altitude was set to 2000m. Path noise was set to 10m for the position and $5e^{-3}$ rad for the orientation. The standard deviation of image noise was set to 0.1 pixels. These values for the path distortion are large compared to the state of the art navigation systems (Sandau, 2010). However, such systems are prohibitively expensive for some users.

The results for 100 runs comparing geometry 1 and 2 are presented in **Table 3**. In this case, the degrees of freedom in the scene geometry do affect the accuracy of BA. The RMS Error is shown in the first two columns. The right two columns contain the shape error. Shape error is computed as the RMS difference between the original terrain and the recovered terrain once it has been shifted and rotated to best match with the original terrain. This measure is not influenced by simple translation or rotation but only by warping as it measures shape deformation.

Reconstructed terrain from the constrained geometry 2 is twice as accurate as the geometry 1 in terms of simple RMS error. In terms of shape error, geometry 2 provides twenty times better reconstruction than geometry 1. These simulations show that geometry can affect terrain reconstruction accuracy for aerial imagery. Moreover the developed method provides a tool for analyzing any geometry and provides insight into the nature of the degrees of freedom.

Even though, we were not able to demonstrate a practical advantage of one geometry over another with aspect ratio's typical to satellites, we were able to demonstrate the effects of geometry on the accuracy of terrain reconstruction under certain limited conditions. Another simulation, more similar to the analysis, with different perturbations on the parameters was performed. In this case, no image noise was added and only one camera pose was disturbed. The other camera's path parameters were left undisturbed and held fixed for BA. In this setup BA was always able to reconstruct the original terrain when geometries without degrees of freedom were used. However, the reconstructed terrain was always deformed with the unconstrained geometries, even though BA cost was reduced to 0. Reasonable values of accuracy for localizing tie points impart so much noise at aspect rations typical to satellites that these errors swamp out the improvements gained using constrained geometry.

To explore the relationship between tie point localization noise and terrain accuracy the termination condition for BA was modified to approximate image noise. Under normal conditions BA runs until it converges (i.e. no better solution can be found). In this investigation, a weaker termination condition dependent upon the cost C was added. BA was stopped after it reached some predefined cost. Since the BA's cost is an aggregate image error, a weak termination condition is similar to feature localization noise. In this case, no image noise is added, but the pose parameters were perturbed. **Table 4** presents results of this simulation for geometry 1, 2 and 4. When the termination condition allows the cost C to be relatively large BA exhibits no dependence on the scene constraints. As the termination condition is reduced, the performance for the constrained geometries improves. Unfortunately, to take advantage of the constraints of the scene, BA has to be able to converge to extremely small cost which on average is a fraction of the size of a pixel. Obtaining such a small cost is impossible with a real imagery, where features are identified with the accuracy up to one tenth of the pixel at best. This fact limits the practical significance of the identified degrees of freedom for the imagery obtained by the satellites.

Table 4. Terrain error as a function of a minimum BA cost.

		BA stop condition - avg. cost per feature						
		1 pixel	*0.1 pixel*	*0.01 pixel*	*$1e^{-3}$ pixel*	*$1e^{-4}$ pixel*	*$1e^{-5}$ pixel*	*0 pixel*
Avg. terrain error - mean(x,y,z)	***Geo 1***	*0.239*	*0.239*	*0.235*	*0.235*	*0.236*	*0.219*	*0.223*
	Geo 2	*0.300*	*0.137*	*0.131*	*0.129*	*0.045*	*0.007*	*0.000*
	Geo 4	*0.216*	*0.217*	*0.217*	*0.217*	*0.127*	*0.015*	*0.000*

CONCLUSIONS

This paper presented a BA formulation for pushbroom cameras. A method for identifying degrees of freedom in viewing geometries was developed. The method based on the decomposition of the Hessian matrix computed at the solution is able to identify linear directions along which the cost remains zero. The method was applied to five commonly used geometries. In two of these cases, certain degrees of freedom were found that should deleteriously affect terrain reconstruction accuracy. Numerical simulations under conditions resembling real camera systems were performed in order to verify expected negative effect of degrees of freedom on BA. It was found that for satellite imagery BA improves the terrain reconstruction similarly for all geometries, regardless of the presence of degrees of freedom in the geometry. Further analysis was able to attribute this discrepancy between theory and practice. For simulations of lower altitude aerial imagery, the geometry did affect terrain reconstruction accuracy particularly with wide FOV imagery.

REFERENCES

Ackermann, F., J. Bodechtel, F. Lanzl, D. Meissner, P. Seige, H. Winkenbach, and J. Zilger (1991, Jun). MOMS-02 a multispectral stereo scanner for the second german spacelab mission D2. In *International Geoscience and Remote Sensing Symposium, 1991. IGARSS '91.*, Volume 3, pp. 1727–1730.

Bouillon, A., M. Bernard, P. Gigord, A. Orsoni, V. Rudowski, and A. Baudoin (2006). Spot 5 hrs geometric performances: Using block adjustment as a key issue to improve quality of dem generation. *ISPRS Journal of Photogrammetry and Remote Sensing 60*(3), 134 – 146. Extraction of Topographic Information from High-Resolution Satellite Imagery.

Brown, D. C. (1958). A solution to the general problem of multi station analytical stereotriangulation. Technical report, Patric Airforce Base, Florida.

DigitalGlobe (2009). QuickBird spacecraft data sheet. Internet. http://www.digitalglobe.com/index.php/85/-QuickBird.

Duff, I. S., A. M. Erisman, and J. K. Reid (1989). *Direct methods for sparse matrices*. New York, NY, USA: Clarendon Press.

Ebner, H., W. Kornus, T. Ohlhof, and E. Putz (1999). Orientation of moms-02/d2 and moms-2p/priroda imagery. *ISPRS Journal of Photogrammetry and Remote Sensing 54*(5-6), 332 – 341.

Ebner, H. and G. Strunz (1988). Combined point determination using digital terrain models as control information. *International Archives of Photogrammetry and Remote Sensing 27*(3), 578–587.

Fletcher, R. (2000). *Practical Methods of Optimization*. Wiley.

Fricker, P. (2001). ADS40 – progress in digital aerial data collection. In *In: D. Fritsch, R. Spiller (Eds.), Photogrammetric Week '01*, Heidelberg. Wichmann Verlag.

George, A. and J. W. Liu (1981). *Computer Solution of Large Sparse Positive Definite*. Prentice Hall Professional Technical Reference.

Gleyzes, J.-P., A. Meygret, C. Fratter, C. Panem, S. Baillarin, and C. Valorge (2003, July). SPOT5: system overview and image ground segment. In *Geoscience and Remote Sensing Symposium, 2003. IGARSS '03. Proceedings. 2003 IEEE International*, Volume 1, pp. 300–302.

Hartley, R. and A. Zisserman (2004). *Multiple View Geometry in Computer Vision.* Cambridge University Press.

Hofmann, O., H. Ebner, and P. Nave (1984). DPS - a digital photogrammetric system for producing digital elevation models and orthophotos by means of linear-array scanner imagery. *Photogrammetric engineering and remote sensing 50*, 1135–1142.

Kirk, R. L., E. Howington-Kraus, M. R. Rosiek, D. Cook, J. Anderson, K. Becker, B. A. Archinal, L. Keszthelyi, R. King, A. S. McEwen, and H. Team (2007). Ultrahigh resolution topographic mapping of Mars with HiRISE stereo images: Methods and first results. In *Seventh International Conference on Mars*.

Korona, J., E. Berthier, M. Bernard, F. Rémy, and E. Thouvenot (2009). SPIRIT. SPOT 5 stereoscopic survey of polar ice: Reference images and topographies during the fourth international polar year (2007-2009). *ISPRS Journal of Photogrammetry and Remote Sensing 64*(2), 204 – 212.

Li, R., J. W. Hwangbo, Y. Chen, and K. Di (2008, July). Rigorous photogrammetric processing of HiRISE stereo images for mars topographic mapping. In *The XXI Congress of the International Society for Photogrammetry and Remote Sensing*, Beijing, China.

Neukum, G. (1999). The airborne HRSC-A: Performance results and application potential. In *In D. Fritsch and R. Spiller (eds) Photogrammetric Week '99*. Wichmann Verlag.

Orun, A. B. and K. Natarajan (1994). A modified bundle adjustment software for SPOT imagery and photography: Tradeoff. *Photograrnmetric Engineering and Remote Sensing 60*(12), 1431–1437.

Salvini, R., M. Anselmi, A. Rindinella, and I. Callegari (2004). Quickbird stereo-photogrammetry for geological mapping (Cyrene-Libya). In *ISPRS Congress Istanbul*.

Sandau, R. (2010). *Digital Airborne Camera*. Springer Netherlands.

Triggs, B., P. Mclauchlan, R. Hartley, and A. Fitzgibbon (2000). Bundle adjustment –- a modern synthesis. In *Vision Algorithms: Theory and Practice, LNCS*, pp. 298–375. Springer Verlag.